International Journal of Fluid Machinery and Systems
Vol. 2, No. 4, October-December 2009

Original Paper

Inducer Design to Avoid Cavitation Instabilities

Donghyuk Kang[1], Toshifumi Watanabe[1], Koichi Yonezawa[1], Hironori Horiguchi[1], Yutaka Kawata[2], Yoshinobu Tsujimoto[1]

[1]Graduate School of Engineering Science, Osaka University
1-3 Machikaneyama, Toyonaka, Osaka, 560-8531, Japan
[2]Faculty of Engineering, Osaka Institute of Technology,
5-16-1 Ohmiya, Asahi, Osaka, Osaka 535-8585, Japan

Abstract

Three inducers were designed to avoid cavitation instabilities. This was accomplished by avoiding the interaction of tip cavity with the leading edge of the next blade. The first one was designed with extremely larger leading edge sweep, the second and third ones were designed with smaller incidence angle by reducing the inlet blade angle or increasing the design flow rate, respectively. The inducer with larger design flow rate has larger outlet blade angle to obtain sufficient pressure rise. The inducer with larger sweep could suppress the cavitation instabilities in higher flow rates more than 95% of design flow coefficient, owing to weaker tip leakage vortex cavity with stronger disturbance by backflow vortices. The inducer with larger outlet blade angle could avoid the cavitation instabilities at higher flow rates, owing to the extension of the tip cavity along the suction surface of the blade. The inducer with smaller inlet blade angle could avoid the cavitation instabilities at higher flow rates, owing to the occurrence of the cavity first in the blade passage and its extension upstream. The cavity shape and suction performance were reasonably simulated by three dimensional CFD computations under the steady cavitating condition, except for the backflow vortex cavity. The difference in the growth of cavity for each inducer is explained from the difference of the pressure distribution on the suction side of the blades.

Keywords: Inducer, Cavitation instability, Tip cavity, CFD computation

1. Introduction

The suppression of cavitation instability is one of the most important issues for the design of reliable turbo pump inducers for rocket engines. Until now, various cavitation instabilities have been identified [1], including cavitation surge, rotating cavitation, and their higher order modes. They cause high dynamic loads on the shaft and the blades.

Various methods have been experimentally investigated to suppress the cavitation instabilities [2-4]. Shimiya et al.[5] have attempted to suppress the cavitation instabilities by using axial grooves and it was found that the occurrence of the cavitation instabilities are closely related with the interaction of the tip cavity with the leading edge of the next blade.

In the previous study [6], the authors investigated the effect of blade geometry on the tip leakage vortex by using a commercial CFD code under the steady noncavitating condition and found new geometries of the inducer, which were considered to be effective to suppress the interaction of tip leakage vortex with the leading edge of next blade.

In the present study, three inducers were designed on the basis of the CFD results of noncavitating flow, and they were tested to examine the effect of the blade geometry on cavitation instabilities. Three dimensional CFD simulations of the cavitating flow of new inducers were carried out and their results were used for the discussions on the mechanism of the suppression of cavitation instabilities

2. Specifications of Inducers

Figure 1 and Table 1 show the leading edge geometry and geometrical properties for inducers tested, respectively. They have three blades with backward leading edge sweep and the diameter of 149.8mm.

2.1 Original Inducer

The backward leading edge sweep angle is 95.2° in the original inducer, as shown in Fig.1(a). The distributions of the blade angle in the chordwise and radial directions are shown in Figs.2(a) and (b), respectively. At the blade tip, the inlet and outlet blade angles are 7.5° and 9.0° respectively. The blade angle $\beta(r)$ is determined by the helical condition of $r\times\tan\beta(r)=R_t\times\tan\beta_t$, where r

Received June 8 2009; revised September 15 2009; Accepted for publication September 15 2009: Review conducted by Prof. Hyung Hee Cho. (Paper number O09019)
Corresponding author: Mr. Donghyuk Kang, kang@me.es.osaka-u.ac.jp

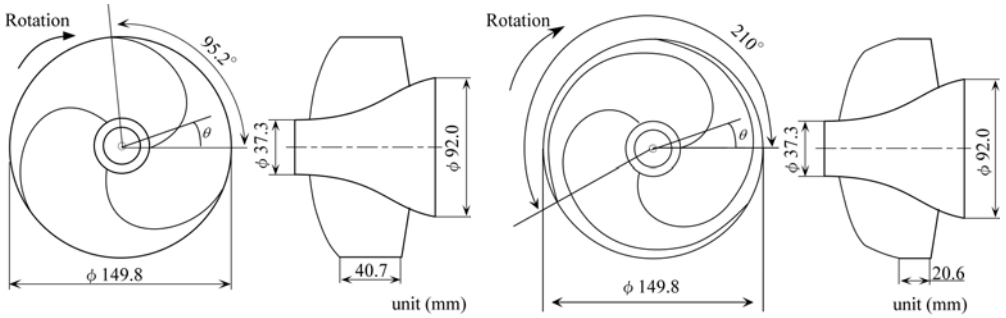

(a) Original inducer, Inducer B and Inducer C

(b) Inducer A

Fig. 1 Leading edge geometry of the inducers

Table 1 Geometrical properties of original inducer and new inducers

	Original inducer	Inducer A	Inducer B	Inducer C
Number of blades	3	←	←	←
Tip diameter (mm)	149.8	←	←	←
Tip clearance (mm)	0.5	←	←	←
Sweep angle (deg)	95.2	210	95.2	←
Inlet tip blade angle (deg)	7.5	←	←	6.0
Outlet tip blade angle (deg)	9.0	←	12.5	9.0
Hub / Tip ratio at inlet	0.25	←	←	←
Hub / Tip ratio at outlet	0.51	←	←	←
Solidity at tip	1.91	0.88	1.91	←
Design flow coefficient, ϕ_d	0.078	←	0.1014	0.078

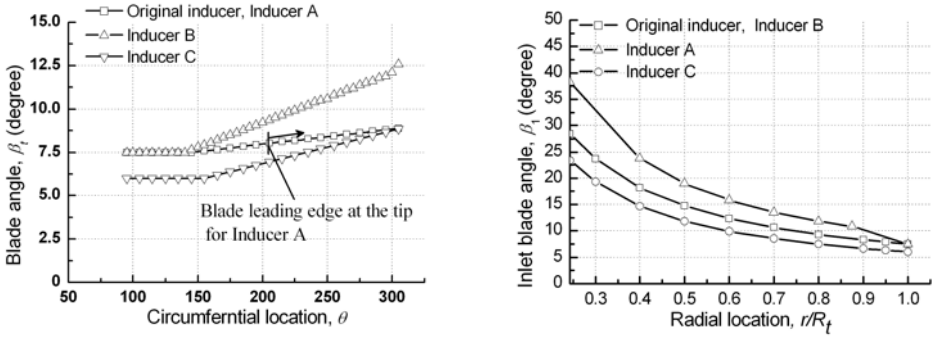

(a) Blade angle at tip

(b) Inlet blade angle

Fig. 2 Distribution of the blade angle in chordwise and radial direction

is the radius, R_t is the radius of the impeller, and β_t is the blade angle at the tip. The design flow coefficient ϕ_d of the original inducer is 0.078. The flow coefficient ϕ is defined as v_1/U_t, where v_1 is the mean axial velocity in the plane at z/D_t=0, and U_t is the tip speed of the inducer. In the present study, ϕ_d=0.078 is used for all inducers as the reference flow coefficient.

2.2 Inducer with Larger Sweep

In experimental and computational results for the original inducer at the design flow coefficient ϕ_d=0.078, the tip vortex starts from the blade leading edge at the tip. This suggests that the interaction of the tip cavity with the leading edge of the next blade would be avoided by moving the starting point of the tip cavity as downstream as possible. Thus, we moved the leading edge of the blade tip downstream by giving a larger sweep. The modified leading edge sweep is shown in Fig.1(b). Firstly, we carried out the simulation of noncavitating flow for an inducer with the modified leading edge sweep but with the same blade angle with the original inducer. Then, a lower pressure region was found at the inner radius of the leading edge. This might cause premature head breakdown due to cavitation. In order to increase the pressure at the lower pressure region, the blade angles at r/R_t=0.875 is increased by 2 °, and linearly decreased to 7.5 ° at the blade tip, as shown in Fig.2(b). The blade angles are changed linearly until θ=150° so that those are equal to the blade angle of the original inducer at θ=150°. It has been reported that the increase of leading edge sweep is effective for the suppression of the cavitation instabilities [4]. This inducer is called "Inducer A"

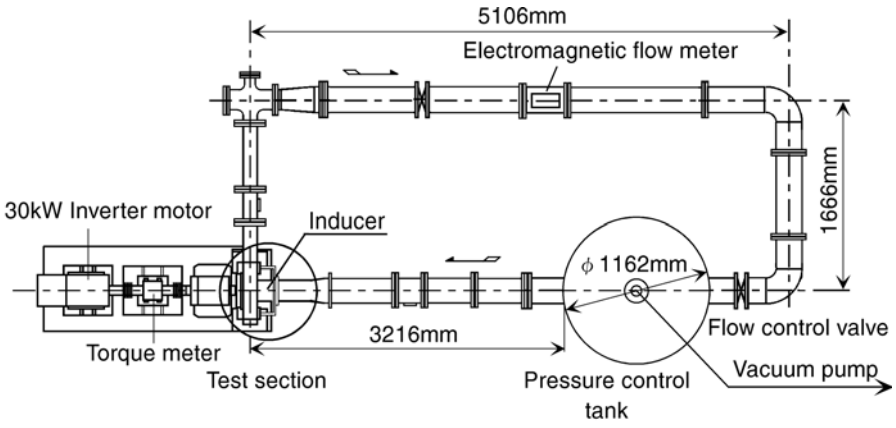

Fig. 3 Test facility

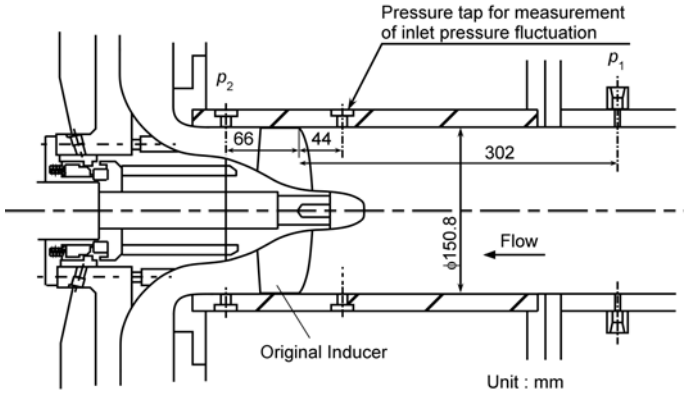

Fig. 4 Test section

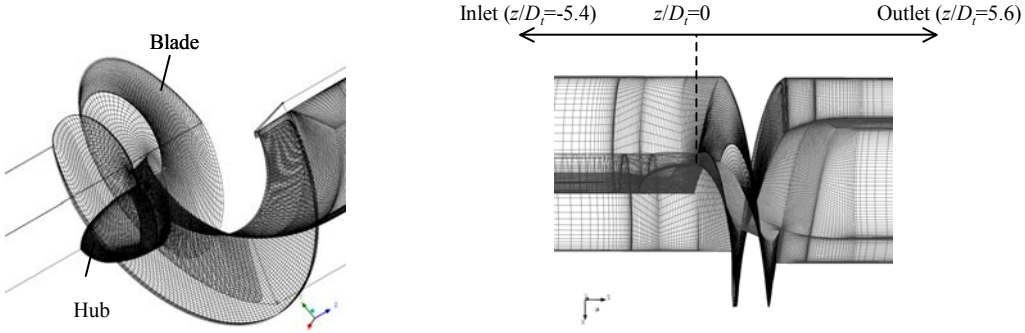

(a) Mesh on the blade and hub (b) Boundaries and z coordinate

Fig. 5 Computational mesh around original inducer

2.3 Inducer with Modified Inlet and Outlet Blade Angles

To avoid the interaction of the tip leakage vortex with the leading edge of the next blade, it is favorable to design the inducer so that the tip leakage vortex extends as parallel as possible to the suction surface. Since the tip leakage vortex separates from the suction surface driven by the leakage flow, decreasing the incidence angle and hence the pressure difference near the leading edge would be helpful. In order to decrease the incidence angle, two methods were applied. One of them is to use the inducer at higher flow rate with the same inlet design. For this purpose, the blade outlet angle is increased so that the inducer can be operated at ϕ/ϕ_d=1.3 with the same pressure rise as the original inducer at ϕ/ϕ_d=1.0. The inducer with larger outlet blade angle is called "Inducer B", and the distribution of the blade angle is shown in Fig. 2(a). At the blade tip, the original blade angle is kept constant up to θ=150°, and linearly increased to the outlet blade angle of 12.5°. The nominal incidence angle λ at ϕ/ϕ_d=1.3 is 1.70°, which is about a half of that of original inducer at ϕ/ϕ_d=1.0, λ=3.04°. The second one is to decrease the inlet blade angle by 1.5° and is called "Inducer C", with the distribution of blade angle shown in Fig. 2(a). The inlet blade angle is 6°, and kept constant up to θ=150° and then linearly increased to the outlet blade angle of 9° which is the same as the original inducer. The nominal incidence angle λ of this inducer at ϕ/ϕ_d=1.0 is 1.54°. For the inducers with the modified outlet and inlet blade angles, the blade angles at all radii were designed based on the helical condition, as shown in Fig. 2(b).

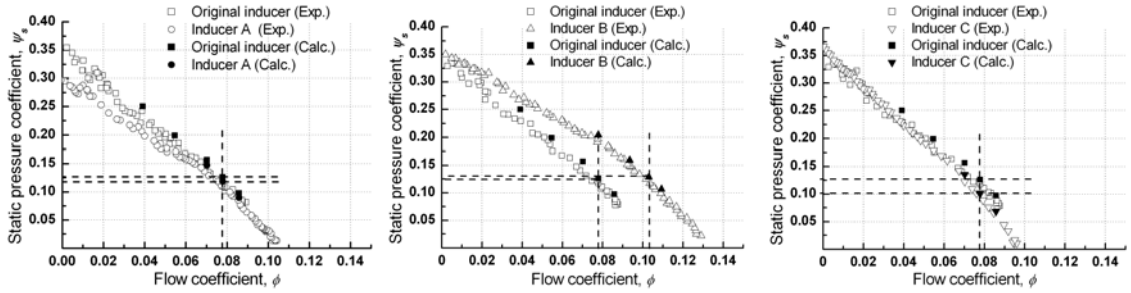

(a) Original inducer and Inducer A

(b) Original inducer and Inducer B

(c) Original inducer and Inducer C

Fig. 6 Performance curves at 1500rpm

3. Experimental and Computational Methods

3.1 Experimental Method

Figure 3 shows the schematic of test facility. The cavitation tunnel is a closed type and the inlet pressure is adjusted by controlling the tank pressure with a vacuum pump and a relief valve. The working fluid is water at room temperature.

Figure 4 shows the details of the test section around the inducer. The inlet and outlet pressures, p_1 and p_2, were measured 302mm upstream and 66mm downstream of the blade leading edge at the tip, respectively. The inlet pressure fluctuations are measured by pressure transducers flush mounted 44 mm upstream of the blade leading edge at the tip. They are installed with circumferential interval of 90° to identify the mode of instabilities. The transducers are strain gauge type (Kyowa PGM-10KC) with the resonance frequency of 40kHz. The casing was made of clear acrylic resin for visual observation.

3.2 Computational Method

A commercial software, ANSYS-CFX11.0, was used for the simulation of the steady cavitating flow of the inducers. The computational mesh around the inducer is shown in Fig.5(a).The flow in one blade channel was calculated by assuming the periodicity. The simplified Reyleigh-Plesset cavitation model and the k-ω turbulence model were used. The working fluids were water and its vapor. The boundaries are shown in Fig.5(b). The number of computational cells is about 2,200,000. Zero circumferential velocity and the total pressure were specified at the inlet and the mass flow rate was specified at the outlet. The rotational speed was fixed at 3000rpm which is the same as the experiments. The axial coordinate z is set in the downstream direction from the origin (z/D_t=0) at the leading edge of blades at root, as shown in Fig.5(b).

4. Results and Discussions

4.1 Performance Curve

Figure 6 shows the noncavitating performance curves obtained from experiments and computations. The static pressure coefficient ψ_s is defined as $(p_2\text{-}p_1)/(\rho U_t^2)$. For Inducer A, the pressure coefficients at lower flow coefficients are lower than those of the original inducer, as shown in Fig.6(a). For Inducer B, the pressure coefficient at ϕ=0.1014 (ϕ/ϕ_d=1.3) is almost the same as that of the original inducer at ϕ=0.078 (ϕ/ϕ_d=1.0), as shown in Fig.6(b). For Inducer C, the negative slope of performance curve is slightly larger than that of the original inducer, as shown in Fig.6(c). Computational results are in agreement with experimental results.

4.2 Occurrence Region of Cavitation Instabilities

Figures 7~9 show the spectra of inlet pressure fluctuations measured by the pressure transducers flush mounted 44mm upstream of the blade leading edge at the tip. The horizontal axis shows the frequency, the vertical axis shows the magnitude of the pressure fluctuation $\Delta\psi$ defined as $\Delta p/(\rho U_t^2)$ and the depth axis shows the cavitation number σ defined as $(p_1\text{-}p_v)/(\rho U_t^2/2)$ where p_v is the vapor pressure. N is the frequency 50Hz of the impeller rotation. For the original inducer, rotating and asymmetric cavitations occurs at all flow rates and cavitation surge is observed in the wide cavitation number at ϕ/ϕ_d=0.9. For Inducer A, a weak cavitation surge is observed but other instabilities can be successfully suppressed at all flow rates. For Inducer B and Inducer C, both rotating cavitation and cavitation surge occur at lower flow rates. However, the broadband component is significantly decreased as compared with original and Inducer A. No cavitation instabilities are found at the design and higher flow rates, except for the weak cavitation surge of Inducer B at the design flow rate of ϕ/ϕ_d=1.3.

Figure 10 shows the regions of various cavitation instabilities on suction performance curves. The nominal incidence angle λ at the tip and the suction performance curve evaluated by CFD are also shown. For Inducer A, cavitation instabilities are suppressed at higher flow rates more than 95% of design flow coefficient except for the cavitation surge at smaller cavitation number. Since the surge occurs in the region where the head is somewhat decreased, this can be a choked surge [7] although no detailed confirmation was made. For Inducer B and Inducer C, no cavitation instabilities are found at the incidence angle less than 1.5°. However, at higher flow rate, the head starts to decrease gradually at higher cavitation number since the cavity starts to occur in the blade passage. These results show that the design method to avoid or reduce the interaction of the tip vortex with the leading edge of the next blade is effective for the suppression of cavitation instabilities. Theoretical background for this was given by three dimensional simulation of alternate blade cavitation, rotating cavitation and cavitation surge [8].

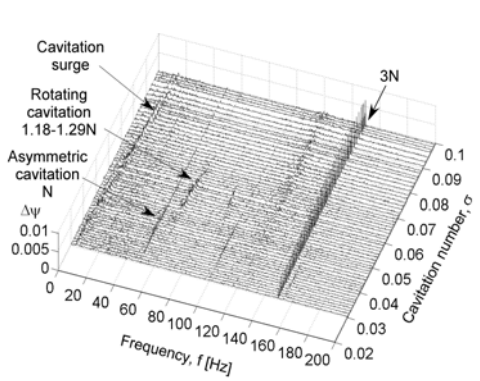

(a) Original inducer at ϕ/ϕ_d=0.9

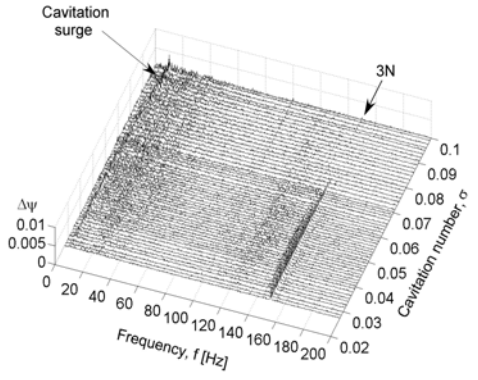

(b) Inducer A at ϕ/ϕ_d=0.9

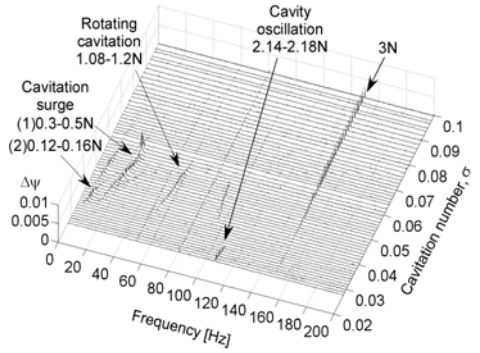

(c) Inducer B at ϕ/ϕ_d=1.2

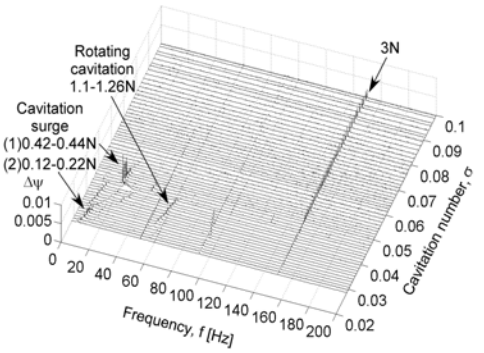

(d) Inducer C at ϕ/ϕ_d=0.9

Fig. 7 Spectra of inlet pressure fluctuations at 3000rpm at lower flow coefficient

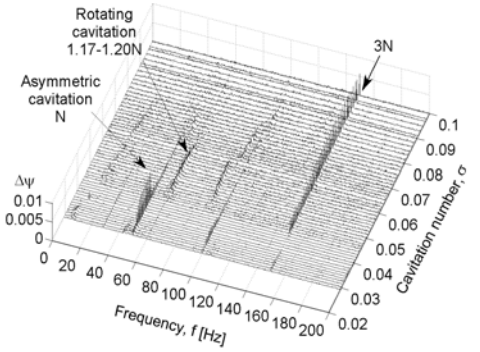

(a) Original inducer at ϕ/ϕ_d=1.0

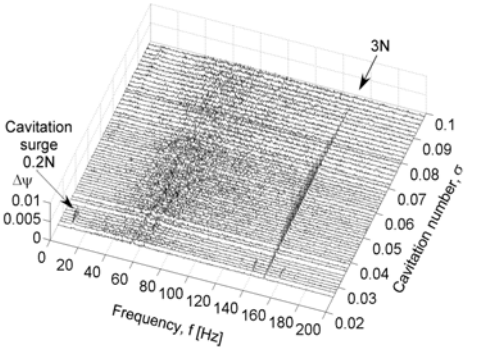

(b) Inducer A at ϕ/ϕ_d=1.0

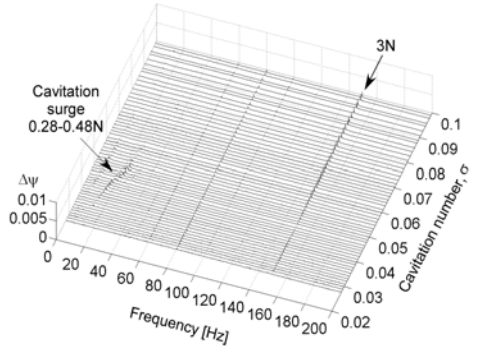

(c) Inducer B at ϕ/ϕ_d=1.3

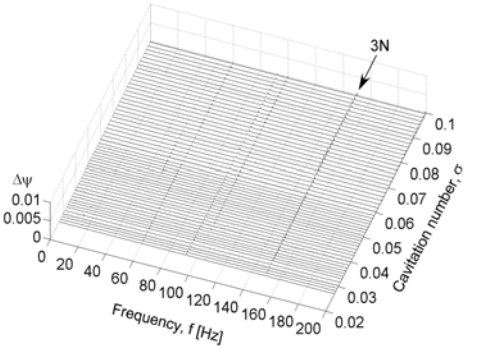

(d) Inducer C at ϕ/ϕ_d=1.0

Fig. 8 Spectra of inlet pressure fluctuations at 3000rpm at the design flow coefficient

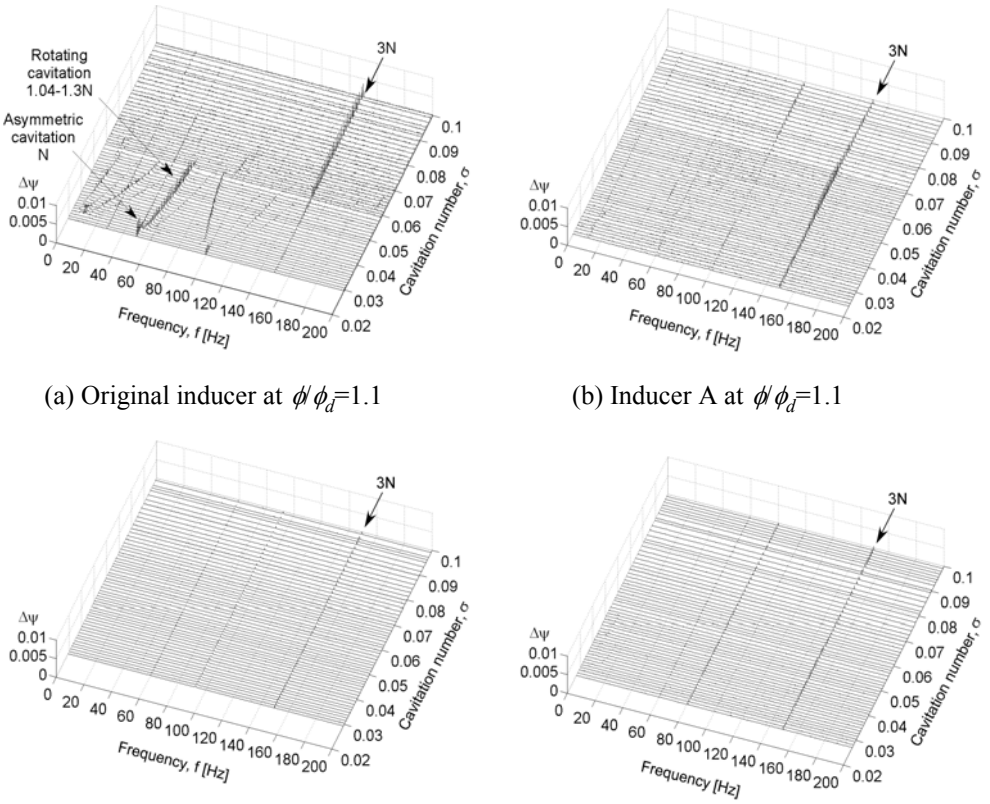

(a) Original inducer at ϕ/ϕ_d=1.1 (b) Inducer A at ϕ/ϕ_d=1.1

(c) Inducer B at ϕ/ϕ_d=1.4 (d) Inducer C at ϕ/ϕ_d=1.1

Fig. 9 Spectra of inlet pressure fluctuations at 3000rpm at higher flow coefficient

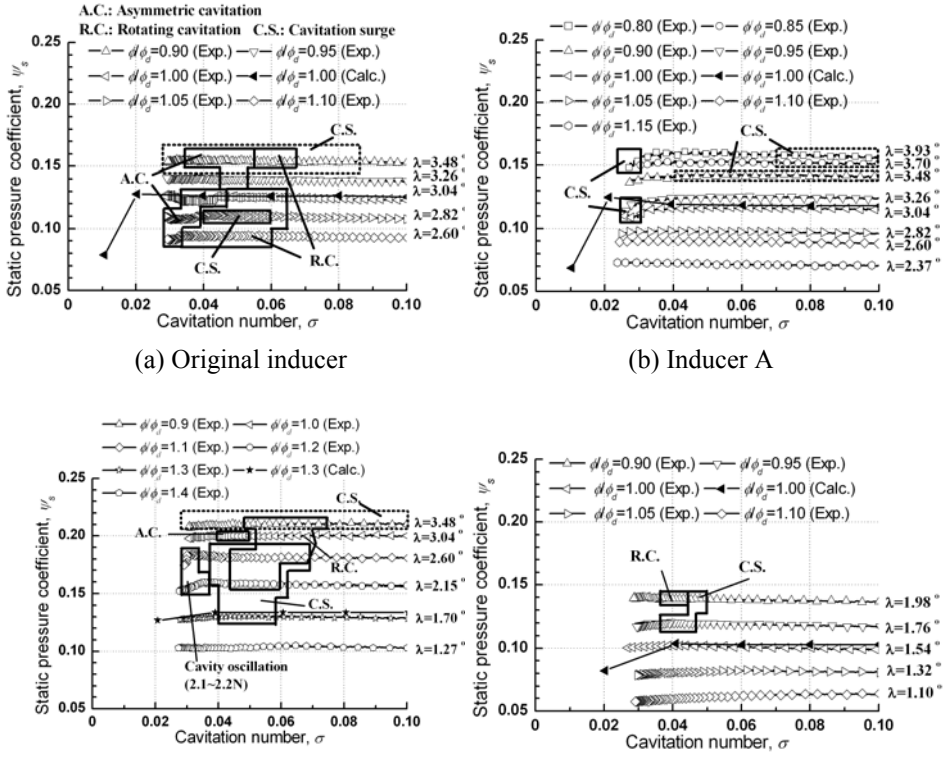

(a) Original inducer (b) Inducer A

(c) Inducer B (d) Inducer C

Fig. 10 Suction performance curves with the occurrence regions of the cavitation instabilities at 3000rpm

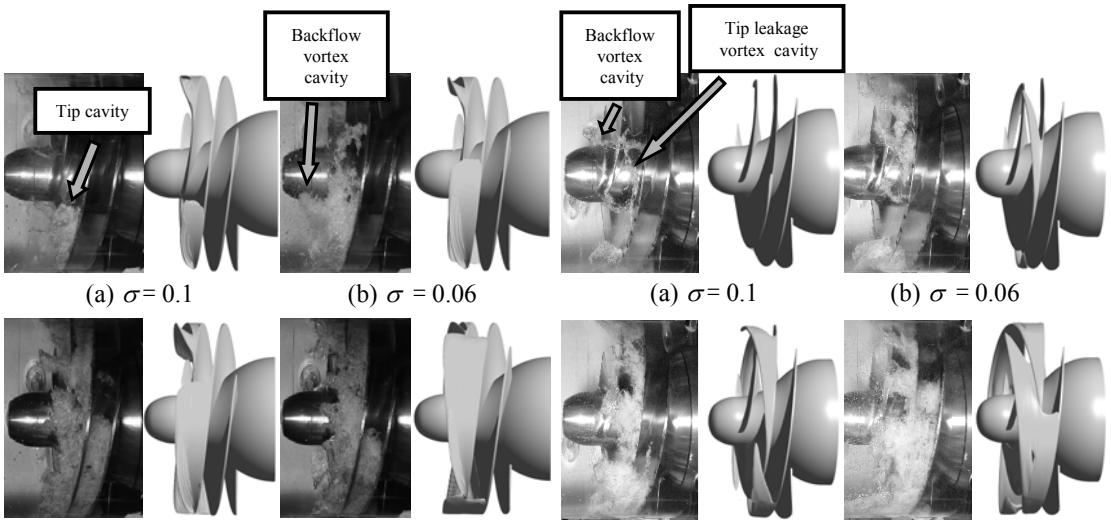

Fig. 11 Cavity shape for the original inducer at ϕ/ϕ_d=1.0, 3000rpm

Fig .12 Cavity shape for Inducer A at ϕ/ϕ_d=1.0, 3000rpm

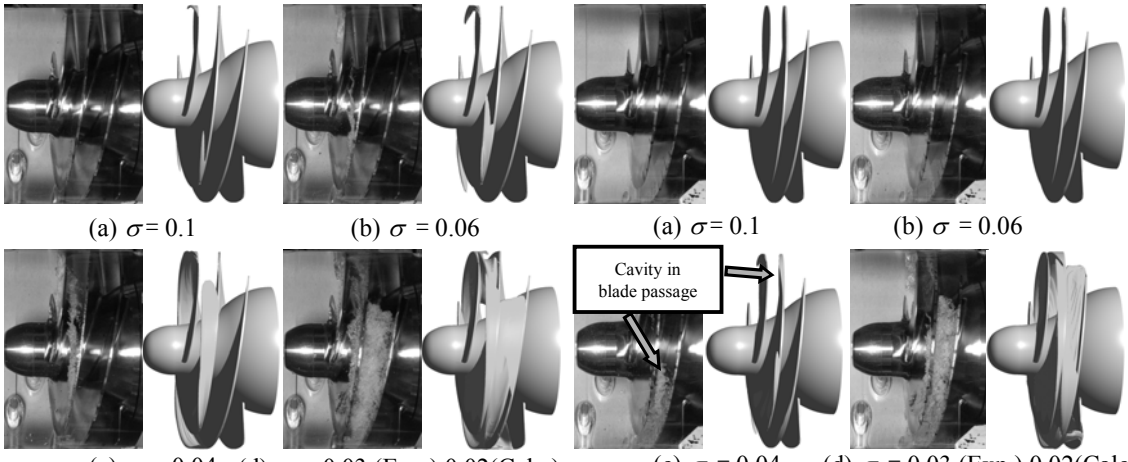

Fig. 13 Cavity shape for Inducer B at ϕ/ϕ_d=1.3, 3000rpm

Fig. 14 Cavity shape for Inducer C at ϕ/ϕ_d=1.0, 3000rpm

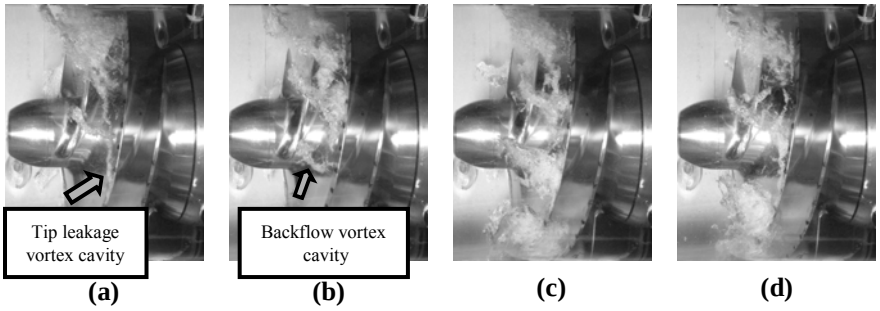

Fig. 15 Cavity shape for Inducer A at 3000rpm, ϕ/ϕ_d=1.0, σ=0.06

4.3 Cavity Shape

Figure 11 shows the cavity shapes for the original inducer obtained from experiments and computations. In computations, the cavity was shown by a plane with the void fraction α=0.01. For the original inducer, the tip cavity extends continuously from the blade tip. So, we simply call it "tip cavity". At σ=0.06, rotating cavitation is observed in experiment and the larger cavity is compared with the result of steady calculation in Fig.11(b). At σ=0.04, an asymmetric cavitation is observed in experiment and the larger cavity is compared with the result of steady calculation in Fig.11(c). The steady computations could simulate the tip cavity reasonably although backflow vortex cavity, rotating cavitation and asymmetric cavitation observed in experiments were not simulated by the steady CFD on one blade channel assuming periodicity.

Figure 12 shows the cavity shapes for Inducer A. The backflow vortex cavity is more clearly observed in experiments as compared with the original inducer. We call the tip cavity "tip leakage vortex cavity " since it occurs in the vortex formed by the roll up the shear layer of the leakage flow. It is somewhat separated from the blade tip, but it extends almost parallel to the blade surface.

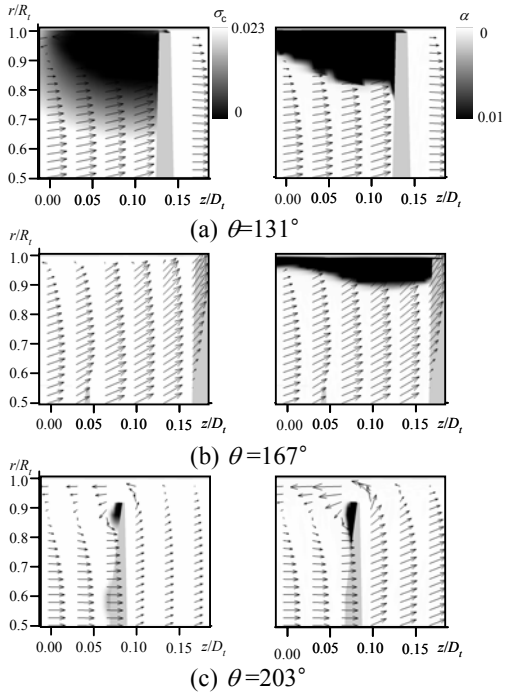

Fig. 16 Velocity vector and local cavitation number and void fraction distribution for the original inducer at ϕ/ϕ_d=1.0, σ=0.04

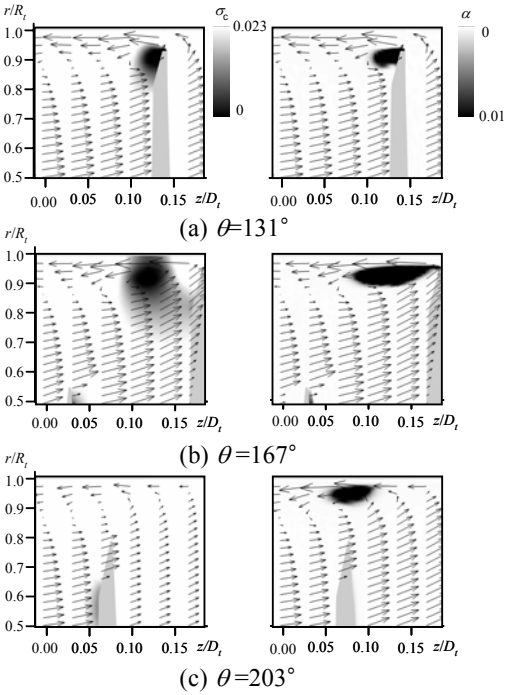

Fig. 17 The same as Fig.16, for Inducer A at ϕ/ϕ_d=1.0, σ=0.04

Figure 13 shows the cavity shapes for Inducer B at ϕ/ϕ_d=1.3. The amount of cavity is remarkably reduced as compared with the original inducer at ϕ/ϕ_d=1.0. The tip leakage vortex cavity extends downstream along the suction side of the blade, as shown in Fig.13(c). The computations could simulate the tip leakage vortex cavity reasonably.

Figure 14 shows the cavity shapes for Inducer C. The tip leakage vortex cavity appear first in the blade passage, as shown in Fig.14(c), and then extends upstream as the cavitation number decreases, as shown in Fig.14(d). The computations could simulate the onset of tip cavity downstream of the throat. The difference of the cavity appearance from Inducer B can be caused by smaller incidence angle.

Figure 15 shows the cavity shapes for Inducer A, taken at different times under the same condition. The isolated tip leakage vortex cavity detached from the blade surface is found and the backflow vortex cavity is clearly observed. These pictures show that the tip leakage vortex cavity is mostly extending along the blade surface but is disturbed by the backflow vortices. Thus, the interaction of tip leakage vortex cavity with the leading edge of the next blade at lower flow rate can occur only intermittently. This is considered to be the reason why the cavitation instabilities can be avoided at all flow rates.

Figures 16 and 17 show the velocity vector, local cavitation number σ_c and void fraction α for the original inducer and Inducer A. The local cavitation number σ_c is defined as $(p\text{-}p_v)/(0.5\rho U_t^2)$. For the original inducer, a large tip cavity occurs at θ=131 ° corresponding to the large low pressure region near the casing, as shown in Fig.16(a). The cavity still exists in the higher pressure region at θ=167 °, as shown in Fig.16(b). This shows that the cavity in θ=167 ° appears in the lower pressure region in θ=131 ° and remains due to the lag of the condensation. For Inducer A, the tip cavity appears only around the tip vortex core, as shown in Figs.17(a) and (b). This explains the difference of the "tip cavity" and " tip leakage vortex cavity" in Figs.11 and 12.

4.4 Cavity Length and Blade Loading

Figure 18 shows the circumferential cavity length l_c normalized by the blade circumferential spacing h. In CFD, the cavity surface is identified from the surface with the void fraction α=0.01 and its length is plotted. Generally l_c is defined as the circumferential distance between the leading edge and the cavity trailing edge at the tip. However, for inducer C, the tip cavity appears in the blade passage first separated from the leading edge. In this case, the location of the cavity trailing edge is plotted.

Rotating cavitation occurred for the original inducer when the cavity length reached l_c/h=0.70. For Inducer B and Inducer C, the slope of l_c/h in σ<0.1 is larger than that of the original inducer, as shown in Figs.18(a) and (b). A weak cavitation surge occurs for Inducer B when the cavity extends into the blade passage, but no other cavitation instabilities are observed. This is because the tip cavity is weak and nearly parallel to the suction surface.

For reference purpose, the cavity length on 4-bladed inducers [2] are shown in Fig.18(c). The blade angles are the same as the original inducer and the effects of leading edge geometry were studied. In all cases, alternate blade cavitation in which the cavity length on each blade differs alternately occurred when the cavity length became larger than 65% of blade circumferential spacing. This agrees with the results of 2-D stability analysis [9] and 3-D CFD [8] and shows that the cavitation instabilities generally occur for conventional inducers when the cavity length becomes 65~70% of the blade circumferential spacing.

For new inducers, cavitation instabilities such as rotating and asymmetric cavitation were successfully suppressed by avoiding the interaction of tip cavities with the next blade even though the cavity length exceeds about 65 % of blade circumferential spacing. This result shows that cavitation instabilities can be suppressed by avoiding the interaction of tip leakage vortex cavitation with the leading edge of next blade.

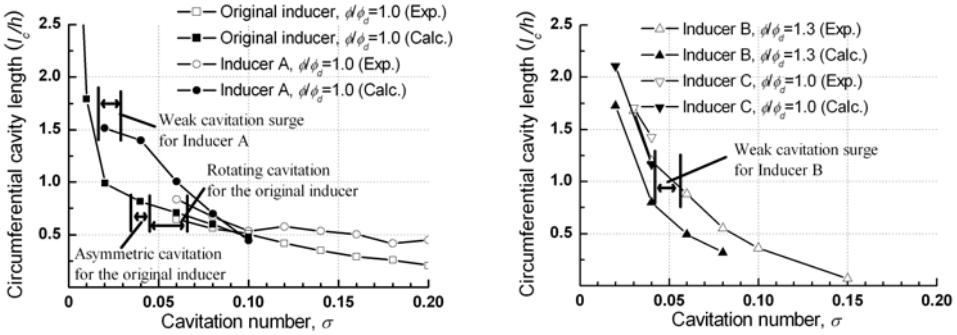

(a) Original inducer and Inducer A (b) Inducer B and Inducer C

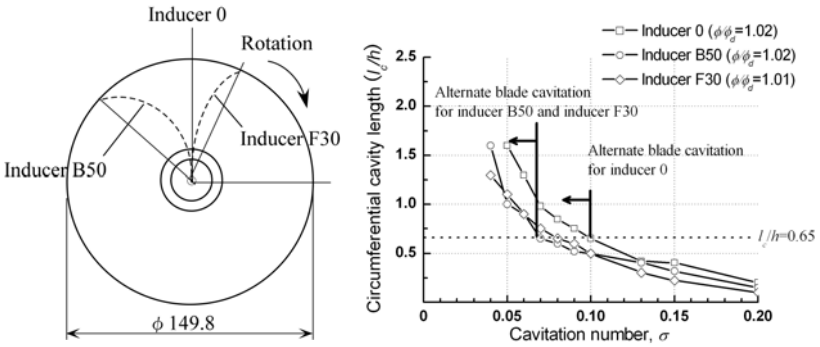

(c) Reference data, from Acosta et al. [2]

Fig. 18 Circumferential cavity length

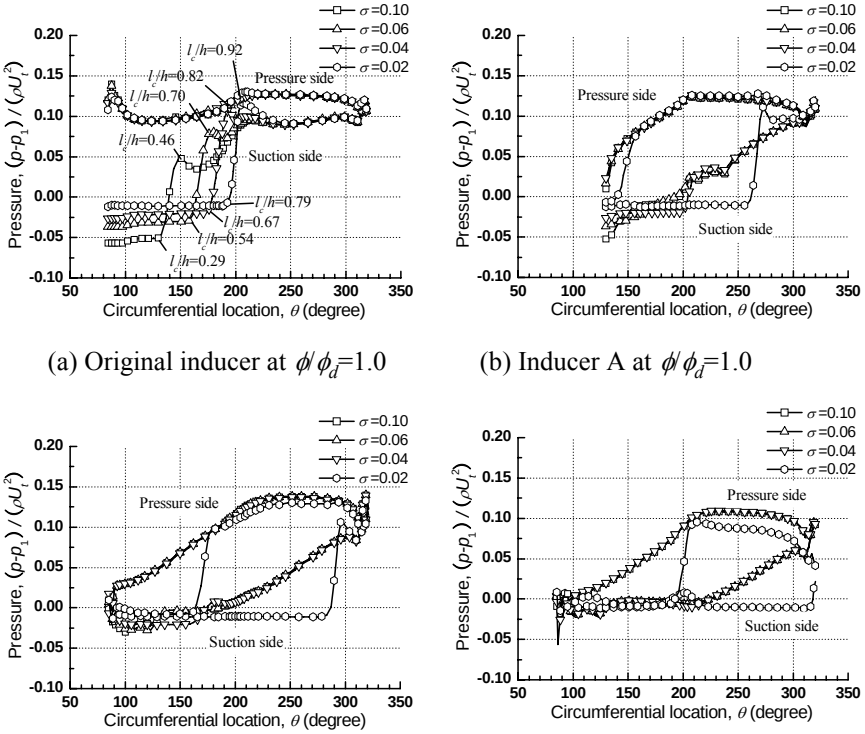

(a) Original inducer at ϕ/ϕ_d=1.0 (b) Inducer A at ϕ/ϕ_d=1.0

(c) Inducer B at ϕ/ϕ_d=1.3 (d) Inducer C at ϕ/ϕ_d=1.0

Fig. 19 Pressure distribution at r/R_t=0.95

Figure 19 shows the pressure distribution on the blade at r/R_t=0.95 from CFD. The horizontal axis shows a circumferential location and the vertical axis shows the pressure defined as $(p\text{-}p_1)/(\rho U_t^2)$. For the original inducer at σ=0.10, the pressure on the suction side near the leading edge is kept nearly constant up to 130° (l_c/h=0.29), and then rapidly rises while θ reaches 150° (l_c/h=0.46). The latter corresponds to the cavity length identified from void fraction shown in Fig.18(a). In the new inducers, the pressure difference near the leading edge is smaller than that of the original inducer and the blade loading is moved downstream. It is interesting that the shift of blade loading occurred also for Inducer A for which the tip blade angle is not changed. This prevents upstream extension of the tip vortex and helps to avoid the interaction of the tip vortex with the next blade. For the original inducer, the pressure on the suction side increases to higher value upstream of the throat at θ=210 °. This is the reason of

the slow growth of the cavity. For the new inducers, the pressure on the suction side gradually increases to the value at the trailing edge. This is the reason of the rapid growth of the cavity.

5. Conclusions

Three inducers were designed for the suppression of cavitation instabilities and the effects of the blade geometry are examined. The results are summarized as follows.

(1) For the inducer with larger sweep, the cavitation instabilities were suppressed in higher flow rates more than 95% of design flow coefficient, owing to the weakening of the tip cavity with stronger disturbance by the backflow vortices.
(2) For the inducer with larger outlet blade angle, the cavitation instabilities at higher flow coefficients were avoided, owing to the extension of tip cavity along the suction surface of the blade.
(3) For the inducer with smaller inlet blade angle, the cavitation instabilities were avoided at higher flow rates, owing to the occurrence of the cavity first in the blade passage and its extension upstream.
(4) Cavitation instabilities could be suppressed with the incidence angle less than 1.5° for all inducers tested.
(5) Avoiding the interaction of tip cavity with the leading edge of the next blade is a good guideline for the suppression of cavitation instabilities.
(6) The commercial code used could reasonably simulate the development of cavitation.

Acknowledgement

Earlier examination of inducer design was carried out with the help of Dr.CEVONE Angelo of Pisa University. The authors would like to thank his contributions. This study was made under the support of Grant-in-Aid for Scientific Research (B)

Nomenclature

D_t	Diameter of inducer [m]	α	Void Fraction
f	Frequency of pressure fluctuation [Hz]	β_t	Blade angle at the tip [degree]
h	Circumferential spacing at the tip [m] = $2\pi R_t /3$	β_1	Inlet blade angles [degree]
l_c	Circumferential cavity length [m]	ϕ	Flow coefficient = v_1/U_t
l_a	Axial cavity location [m]	ϕ_d	Design flow coefficient =0.078
N	Frequency of impeller rotating [Hz]	λ	Incidence angle [degree]
p_1	Pressure at the inlet [Pa]	θ	Circumferential location [m]
p_2	Pressure at the outlet [Pa]	ρ	Density of water [kg/m^3]
p_v	Vapor pressure [Pa]	σ	Cavitation number =$(p_1-p_v)/(\rho U_t^2/2)$
r	Radial location [m]	σ_c	Local cavitation number =$(p-p_v)/(\rho U_t^2/2)$
R_t	Radius of inducer [m]	ψ_s	Pressure coefficient =$(p_2-p_1)/(\rho U_t^2)$
U_t	Tip speed [m/s]	$\Delta\psi$	Fluctuating pressure coefficient =$\Delta p/(\rho U_t^2)$
v_1	Mean axial velocity at the inlet (z/D_t=0) [m/s]		
z	Axial location measured from the root of the leading edge [m]		

References

[1] Tsujimoto, Y., Horiguchi, H., Fujii, A., 2004, "Non-Standard Cavitation Instabilities in Inducers," Proceedings of the 10th International Symposium on Transport Phenomenon and Dynamic of Rotating Machinery, ISROMAC10-2004-020, pp. 1-11.
[2] Acosta, A, Tsujimoto, Y., Yoshida, Y., Azuma, S., 2001, "Effects of Leading Edge Sweep on the Cavitation Characteristics of Inducer Pumps," International Journal of Rotating Machinery, Vol. 7, No. 6, pp. 397-404.
[3] Kamijo, K., Yoshida, M., Tsujimoto, Y., 1993, "Hydraulic and Mechanical Performance of LE-7 LOX Pump Inducer," Journal of Propulsion and Power, Vol. 9,No. 6, pp. 819-826.
[4] Fujii, A., Mizuno, S., Horiguchi, H., Tsujimoto, Y., 2005, " Suppression of Cavitation Instabilities by Jet Injection at Inducer Inlet," Proceeding of the ASME 2005 Fluid Engineering Division Summer Meeting, FEDSM2005-77380, pp. 1477-1482.
[5] Shimiya, N., Fujii, A., Horiguchi, H., Uchiumi, M., Kurokawa, J., and Tsujimoto, Y., 2008, "Suppression of Cavitation Instabilities in an Inducer by J-Groove," ASME Journal of Fluids Engineering, Vol. 130, No. 1, pp. 021302-1-021302-7.
[6] Kang, D., Cervone, A., Yonezawa, K., Horiguchi, H., Kawata, Y., Tsujimoto, Y., 2007, "Effect of Blade Geometry on Tip Leakage Vortex of Inducer," Proceeding of the 9th Asian International Conference on Fluid Machinery, AICFM9-042, pp. 1-6.
[7] Watanabe, T., Kang, D., Cervone, A., Kawata, Y., and Tsujimoto, Y., 2008, "Choked Surge in a Cavitating Turbopump Inducer," International Journal of Fluid Machinery and Systems, Vol. 1, No. 1, pp. 64-75.
[8] Kang, D., Yonezawa, C., Horiguchi, H., Kawata, Y., and Tsujimoto, Y., 2009, "Cause of Cavitation Instabilities in Three-Dimensional Inducer," International Journal of Fluid Machinery and Systems, Vol. 2, No. 3, pp. 206-214.
[9] Horiguchi,H.,Watanabe,S.,Tsujimoto,Y. and Aoki, M., 2000, "Theoretical Analysis of Alternate Blade Cavitation in Inducers," ASME Journal of Fluids Engineering, Vol. 122, No. 1, pp. 156-163.